CHAPTER IV
RESULTS AND DISCUSSION

The first section of this chapter provides the information of process description and key process simulation specification of MEA-based CO_2 capture process. Section 4.2 focuses on screening ionic liquids which have the potential to capture CO_2 from post combustion flue gas. The major factors of consideration are its capture capacity of IL. Section 4.3 focuses on the method to define physical properties, thermodynamic properties and equilibrium calculation of chosen IL into the Aspen Plus. Section 4.4 provides information of process description and key process specification of IL-based CO_2 capture process. The comparison of both processes is discussed in last section.

4.1 MEA-based CO_2 Capture Process

4.1.1 Process Description

The CO_2 capture units in this thesis are simulated to capture CO_2 based on the flue gas from 180 MWe coal burning power plant (flue gas flow rate of 32 tons/h, gas composition of 84 % N_2, 12 % CO_2, and 4 % water vapor per standard volume). The MEA-based CO_2 capture process is designed to meet the target of 90 % capture capacity with 98 % purity of CO_2 by using 25 wt% MEA.

Table 4.1 Post-combustion flue gas composition used

Temperature (°C)	46.1
Pressure (kPa)	115.1
Vapor Fraction	1.0
Composition (mol %)	
N_2	77.93
CO_2	13.14
H_2O	8.92

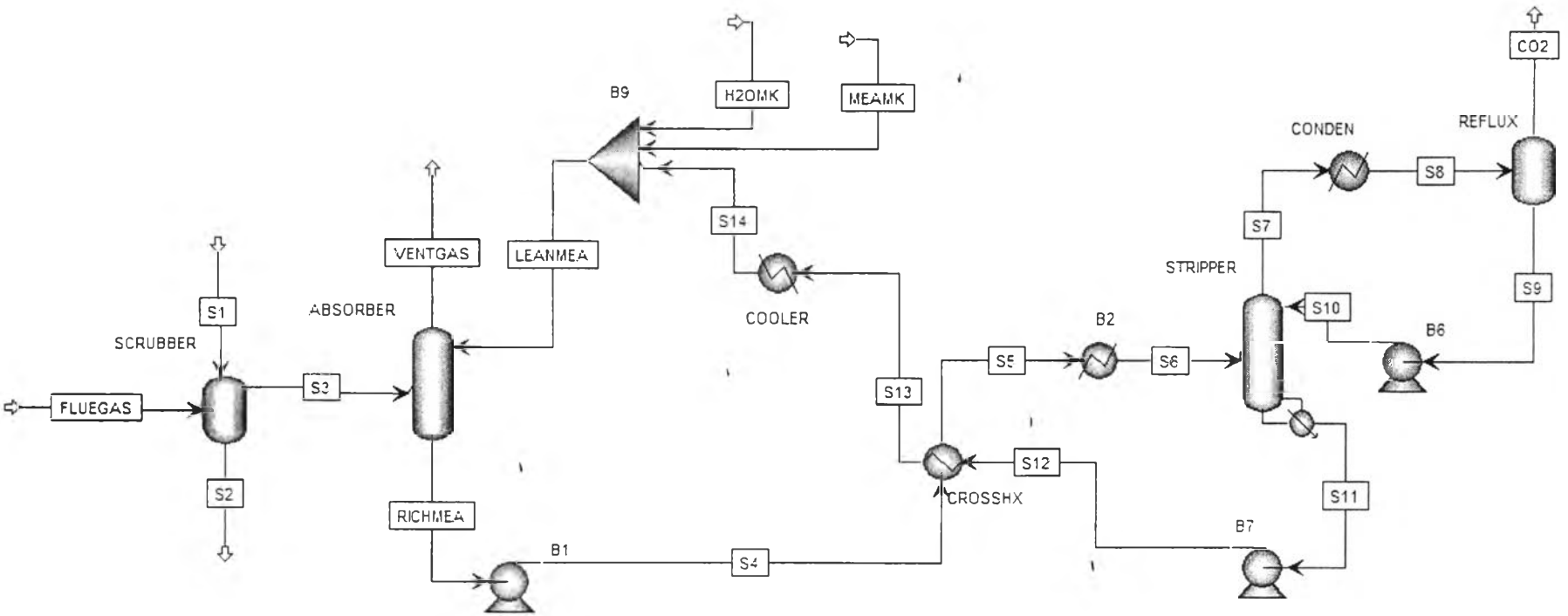

Figure 4.1 MEA-based CO_2 capture flow diagram by Aspen Plus simulation.

Table 4.2a Stream summary of MEA-based CO_2 capture process

Stream	CO2	FLUEGAS	H2OMK	LEANMEA	MEAMK	RICHMEA	S1
Temperature (^{O}C)	30	142	35	35	35	51.7	30
Pressure (bar)	1	11.146	1.358	1.358	1.358	1.013	1.289
Vapor Fraction	1	1	0	0	0	0	0
Solid Fraction	0	0	0	0	0	0	0
Mole Flow (kmol/hr)	137.608	1044.899	46.736	6533.68	0.021	6493.086	100.713
Mass Flow (kg/hr)	5901.685	31297.87	841.96	150422.7	1.3	155481.2	1814.369
Volume Flow (cum/hr)	3451.249	3231.021	0.847	154.852	0.001	163.887	1.822
Enthalpy (Gcal/hr)	-12.72	-14.685	-3.184	-462.197	-0.001	-472.259	-6.871
Mole Flow (kmol/hr)							
H2O	5.928	31.347	46.736	5935.623	0	5863.532	100.713
CO2	131.66	146.286	0	0	0	0.212	0
N2	0.021	867.266	0	0	0	0.021	0
MONOE-01	0	0	0	265.76	0.021	35.184	0
MEA+	0	0	0	168.041	0	298.45	0
H3O+	0	0	0	0	0	0	0
MEACOO-	0	0	0	158.015	0	258.16	0
HCO3-	0	0	0	2.438	0	34.761	0
OH-	0	0	0	0.02	0	0.002	0
CO3--	0	0	0	3.784	0	2.764	0

Table 4.2b Stream summary of MEA-based CO_2 capture process

Stream	S2	S3	S4	S5	S6	S7	S8
Temperature (^{O}C)	46.1	46.1	51.8	75	89	87.7	30
Pressure (bar)	1.151	1.151	2.392	2.392	2.392	1.73	1
Vapor Fraction	0	1	0	0	0	1	0.695
Solid Fraction	0	0	0	0	0	0	0
Mole Flow (kmol/hr)	32.799	1112.813	6493.087	6494.211	6496.502	197.944	197.929
Mass Flow (kg/hr)	590.932	32521.31	155481.2	155481.2	155481.2	6990.459	6990.459
Volume Flow (cum/hr)	0.597	25627.71	163.883	165.939	169.239	3407.601	3452.343
Enthalpy (Gcal/hr)	-2.228	-19.327	-472.252	-469.369	-467.575	-16.108	-16.838
Mole Flow (kmol/hr)							
H2O	32.797	99.263	5863.526	5859.581	5858.271	66.203	66.189
CO2	0.002	146.284	0.213	1.338	3.628	131.705	131.691
N2	0	867.266	0.021	0.021	0.021	0.021	0.021
MONOE-01	0	0	35.194	42.661	49.018	0.014	0
MEA+	0	0	298.446	296.05	293.293	0	0.014
H3O+	0	0	0	0	0	0	0
MEACOO-	0	0	258.153	253.083	249.484	0	0
HCO3-	0	0	34.77	39.987	41.764	0	0.014
OH-	0	0	0.002	0.002	0.002	0	0
CO3--	0	0	2.761	1.489	1.021	0	0

Table 4.2c Stream summary of MEA-based CO_2 capture process

Stream	S9	S10	S11	S12	S13	S14	VENTGAS
Temperature (^{O}C)	30	30.1	116.4	116.4	94	35	54.4
Pressure (bar)	1	2.392	1.73	1.358	1.358	1.358	1.013
Vapor Fraction	0	0	0	0	0	0	1
Solid Fraction	0	0	0	0	0	0	0
Mole Flow (kmol/hr)	60.321	60.321	6487.246	6487.246	6486.984	6486.923	1022.06
Mass Flow (kg/hr)	1088.774	1088.774	149579.5	149579.5	149579.5	149579.4	27465.64
Volume Flow (cum/hr)	1.094	1.094	163.171	163.169	160.026	154.005	27446.73
Enthalpy (Gcal/hr)	-4.118	-4.118	-448.728	-448.729	-451.612	-459.012	-9.263
Mole Flow (kmol/hr)							
H2O	60.261	60.261	5886.54	5886.54	5888.123	5888.929	140.11
CO2	0.031	0.031	0.321	0.321	0.059	0	14.631
N2	0	0	0	0	0	0	867.289
MONOE-01	0	0	272.078	272.077	269.588	265.72	0.03
MEA+	0.014	0.014	164.372	164.372	165.014	168.017	0
H3O+	0	0	0	0	0	0	0
MEACOO-	0	0	155.344	155.345	157.192	158.057	0
HCO3-	0.014	0.014	8.135	8.134	6.172	2.419	0
OH-	0	0	0.019	0.019	0.021	0.02	0
CO3--	0	0	0.437	0.437	0.815	3.761	0

The flue gas goes through the scrubber to cool down the temperature to 46 °C with the pressure near atmospheric pressure (115.1 kPa) that is appropriate to the absorber. The flue gas enters the bottom of the absorber, and the lean MEA (25 wt%) with a CO_2 loading of 0.2 mol CO_2/mol MEA enters the top of the column, at pressure 135.8 kPa and 35 °C. The number of stages for the absorber column in this study is 25 to achieve a rich amine loading of 0.36 mol CO_2/mol MEA and 90 % recovery. Vent gas from the top of absorber consists of CO_2 less than 0.02 vol. %. The rich amine from the bottom of the absorber goes to the rich amine pump to increase the pressure to 239.2 kPa. Then it goes to rich/lean heat exchanger with a temperature approach 5 °C to exchange the duty with the hot stream that comes out the stripper column. The rich amine is heated by the stripper pre-heater to the temperature close to the stripper operating temperature (116.4 °C) and enters at the top of the stripper column. In this study, the stripper has 24 stages. In the stripper, the rich solution flow downward against the hot stream from the reboiler. CO_2 is thereby stripped off from the solvent with purity of 98.2 %. The lean solution from the bottom of the stripper is cooled down to 35 °C, and recycled back to the top of the absorber to complete the loop.

$$\text{Loading} = \frac{[CO_2] + [HCO_3^-] + [CO_3^{2-}] + [MEACOO^-]}{[MEA] + [MEA^+] + [MEACOO^-]} \quad (4.1)$$

Loading is an important parameter that affects the energy performance of MEA-based process, referring to mol of CO_2 carrying species over mol of MEA carrying species as displayed in Equation 4.1. The MEA-based process is optimized to minimize energy consumption by varying MEA mass flow rate and MEA loading. In this study, the MEA mass flow rate and loading of the solution that minimize the energy consumption are 41.78 kg/s and 0.2, respectively.

4.1.2 Key Process Simulation Specifications

A summary of simulation inputs are displayed in Table 4.3.

Table 4.3a MEA-based CO_2 capture plant key process simulation specifications

FLUEGAS (Post-combustion Flue Gas Stream)	Temperature (°C)	142
	Pressure (kPa)	115.1
	Molar Flow (kmol/hr)	1044.9
	Composition (mole fraction)	
	N_2	0.83
	CO_2	0.14
	H_2O	0.03
	MEA	-
S3 (Flue Gas Stream from Scrubber)	Temperature (°C)	46.1
	Pressure (kPa)	115.1
	Molar Flow (kmol/hr)	1112.81
	Composition (mole fraction)	
	N_2	0.78
	CO_2	0.13
	H_2O	0.09
LEANMEA (Lean Amine Stream)	Temperature (°C)	35
	Pressure (kPa)	135.8
	Molar Flow (kmol/hr)	6533.77
	Composition (mole fraction)	
	N_2	6.73E-06
	CO_2	-
	H_2O	0.908459
	MEA	0.040674
	MEA^+	0.025719
	$H3O^+$	0
	$MEACOO^-$	0.024186

Table 4.3b MEA-based CO_2 capture plant key process simulation specifications

ABSORBER (Absorber)	Number of Stages	25
	Pressure (kPa)	101.3
	CO_2 Removal (%)	91.67
	Rich Amine Loading	0.36
B1 (Rich Amine Pump)	Outlet Pressure (kPa)	239.2
CROSSHX (Rich/Lean HEX)	Hot Side Outlet Temperature (°C)	94
	Cold Side Outlet Temperature (°C)	75
	Temperature Approach (°C)	5
B2 (Stripper Pre-heater)	Temperature (°C)	89
	Pressure (kPa)	239.2
STRIPPER (Stripper)	Number of Stages	24
	Pressure (kPa)	173
	Reboiler Temperature (°C)	116.4
	Lean Amine Loading	0.2
CO_2 (CO_2 Outlet Stream)	Temperature (°C)	30
	Pressure (kPa)	101.3
	Molar Flow (kmol/hr)	137.61
	Composition (mole fraction)	
	N_2	0.000153
	CO_2	0.956769
	H_2O	0.043079
	MEA	-
CONDEN (Condenser)	Temperature (°C)	30
REFLUX (Reflux Tank)	Temperature (°C)	30
	Pressure (kPa)	101.3

Table 4.3c MEA-based CO_2 capture plant key process simulation specifications

B6 (Reflux Pump)	Outlet Pressure (kPa)	239.2
B7 (Lean Amine Pump)	Outlet Pressure (kPa)	135.8
MEAMK (MEA Makeup Stream)	Temperature (°C)	35
	Pressure (kPa)	135.8
	Molar Flow (kmol/hr)	0.021
	Composition (mole fraction)	
	MEA	1
H2OMK (Water Makeup Stream)	Temperature (°C)	35
	Pressure (kPa)	135.8
	Molar Flow (kmol/hr)	46.74
	Composition (mole fraction)	
	H_2O	1
COOLER	Outlet Temperature (°C)	35

4.2 Screening ILs for CO_2 Capture Process

The gaseous solubility in any solvent is a crucial role in solvent selection for CO_2 capture. Ionic liquids are, in general, physical solvents for capturing CO_2. The CO_2 absorption performances of each IL are not equal for every type of ILs, these performances depend on many factors such as different combination between cation and anion (structural variation); effect of alkyl chain length, effect of substituted group and many others. However, CO_2 solubility in ILs are quite high compared to other gases in post combustion flue gas; therefore, the selectivity for removing CO_2 is quite good. As a result, ILs that physically dissolved CO_2 are attractive for natural gas sweetening and pre-combustion gas separation. However, large scale application of physical ILs for CO_2 capture from flue-gas is mainly hindered by the low CO_2 absorption capacity at post-combustion conditions. The partial pressure of CO_2 at post-combustion conditions is rather low (7-16 mol %), hence CO_2 solubility is lower than 5 mol % even for the best physical

ILs. To overcome this problem, the amine functional group is included into the IL that could greatly improve absorption capacity by reacted with CO_2 (functionalized ionic liquid). These types of ILs are known in another name "task-specific ionic liquid" (TSIL). However, the big problem of these ILs is they get high viscosity after reacting with CO_2 and cannot be operated in the real process (Sanchez *et al.*, 2007). Another option is to use non-functionalized IL or conventional IL that can chemically absorbs CO_2; 1-ethyl-3-methylimidazolium acetate ([emim][Ac]).

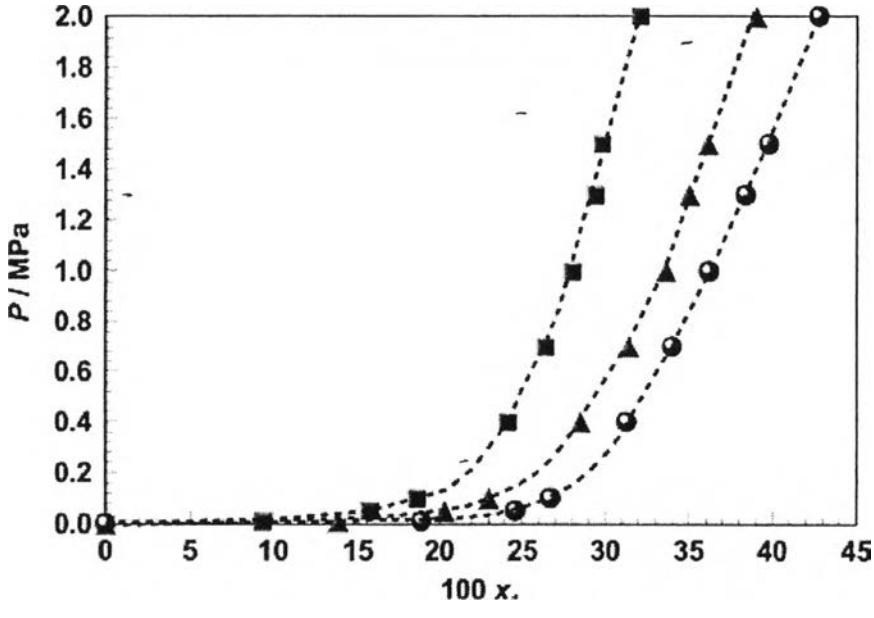

Figure 4.2 The experimental P-x phase diagram of CO_2 + [emim][Ac] at three iso-therm, 298.1 ,323.1 , and 348.1 K; circle, triangle, and square, respectively. x is the mol fraction of CO_2 dissolve in [emim][Ac].

Referring to the experimental study of Shiflett *et al* (2009), they found that CO_2 is strongly chemically absorbed in the IL 1-ethyl-3-methylimidazolium acetate ([emim][Ac]), which is similar to their previous work on the IL 1-butyl-3-methylimidazolium acetate ([bmim][Ac]). IL [emim][Ac] shows highly unusual phase behavior, at low CO_2 concentration (less than 20 mol % of CO_2 at all isotherm), the binary mixtures do not have high vapor pressures, giving a strong attractive (or complex formation) interaction between the CO_2 and [emim][Ac]. The absorption-desorption experiment was done to show that the complex is

reversible. They concluded that this behavior is similar to what they have previously describe for the CO_2 and [bmim][Ac] system, where a highly asymmetric phase behavior with respect to concentration was reported. Such a phase behavior is extremely rare. Furthermore, reversible complex formation of AB_2 (A = CO_2 and B = [bmim][Ac]) was reported for the strong absorption. In the present case, they conclude that the CO_2 (A) and [emim][Ac] (B) are also forming a complex (AB_2) (Yokozeki *et al.*, 2008) by a Lewis acid base reaction.

Based on the study of Shiflett *et al.* (2009), IL [emim][Ac] shows the potential as absorbent for CO_2 capture from post-combustion flue gas (low partial pressure of CO_2). Therefore, the simulation of this CO_2 capture process is studied and compared to the results with the conventional organic solvent (MEA). The main reason of selecting this IL is due to its remarkable absorption behavior and the availability of experimental data.

4.3 Defining Ionic Liquid in the Aspen Plus

4.3.1 Critical Properties of Ionic Liquid [emim][Ac]

Normally, when performing the simulation using Aspen Plus, the properties parameters of selected components will be automatically retrieved. Since the databases of Aspen Plus do not provide any pure component data for [emim][Ac], the direct input information and data regression mode in Aspen Plus are essentially employed. To use the data regression mode for examining the binary interaction parameters of equations of state and activity coefficient model or doing any simulation, the critical properties of selected components are required. Since, the critical properties of ILs are not available and difficult to measure experimentally because it will decompose at the temperature near their normal boiling point. The extended group contribution method, which is called "the modified Lydersen-Joback-Reid" method, is used to estimate the critical properties of IL [emim][Ac]. The reason of selection this method was proven to give good results for molecules of high molecular weight and this method is relatively simple because it requires a basic knowledge of molecular structure and molecular weight (Valderrama and Robles, 2007). This group contribution method also used to estimate the other pure

component properties of IL that are essential to do the simulation such as Heat of formation, Gibbs Energy of Formation and Heat of Vaporization (at normal boiling point). The estimated properties includes normal boiling temperature (T_b), critical temperature (T_c), critical pressure (P_c), critical volume, the acentric factor (ω), heat of formation (H_{form}), Gibbs Energy of Formation (G_{form}), and heat of Vaporization (H_{vap}) of IL [emim][Ac] are shown in Table 4.4.

Table 4.4 Pure component properties of ionic liquid [emim][Ac]

Properties	Value	Properties	Value
Molecular weight (Mw)	170.21	Acentric factor (ω)	0.5492
Boiling temperature (T_b), K	568.21	Heat of formation (H_{form}), kJ/mol	-402.31
Critical temperature (T_c), K	797.85	Gibbs energy of formation (G_{form}), kJ/mol	-177.77
Critical pressure (P_c), bar	29.143	Heat of vaporization (H_{vap}), kJ/mol	54.966
Critical volume (cm^3/mol)	561.00		

Since, no experimental critical properties were available to evaluate the accuracy of the estimated value, the liquid density of IL [emim][Ac] is determined as a consistency test for the predicted properties by using a generalized correlation based on the equation of Spencer and Danner Equation 2.5 and 2.6.

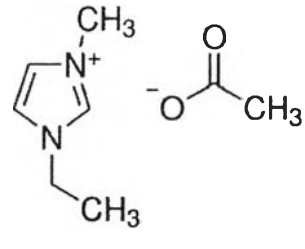

Figure 4.3 Molecular structure of ionic liquid [emim][Ac].

The experimental liquid density of IL [emim][Ac] is brought from the study of Hugo *et al.* (2012). They measured thermo-physical properties of five acetate-based ionic liquid, specifically, density, viscosity, refractive index, and surface tension. The density of IL [emim][Ac] was measured in the temperature range of 283.15 to 363.15 K. The comparison of the experimental and estimated density values are shown in Table 4.5. In this work, the average absolute deviation (AAD) between the experimental and estimated density of IL [emim][Ac] is 0.21 %, which is in the acceptable range of error. So, these pure component and critical properties from the estimation of [emim][Ac] can be used in the simulation.

Table 4.5 Experimental and estimated density of ionic liquid [emim][Ac]

Temperature (K)	**ρexp (g/cm3)**	**ρcal (g/cm3)**	**%Δρcal**
283.15	1.0472	1.156163	10.40518
288.15	1.0429	1.152037	10.46478
293.15	1.0385	1.147897	10.53415
298.15	1.0342	1.143743	10.59203
303.15	1.0299	1.139574	10.64898
308.15	1.0256	1.13539	10.70495
313.15	1.0213	1.131191	10.75992
318.15	1.017	1.126977	10.81385
323.15	1.0127	1.122747	10.86668
328.15	1.0084	1.118501	10.9184
333.15	1.0041	1.114239	10.96895
338.15	0.9998	1.109961	11.01828
343.15	0.9958	1.105666	11.03290
348.15	0.9915	1.101353	11.07952
353.15	0.9872	1.097024	11.12478
358.15	0.9828	1.092677	11.17996
363.15	0.9785	1.088311	11.22242
		AAD (%)	0.214398

4.3.2 Temperature-dependent Properties

Same with the critical properties of IL, Aspen Plus does not provide any thermo-physical properties of IL. Therefore, the experimental data from the literature have to be input into the Aspen Plus in form of parameters called "temperature-dependent correlation parameter". Regression mode in Aspen Plus is employed for this purpose. The properties of IL at various temperatures are correlated as a function of temperature with each property's equation installed in Aspen Plus. The temperature-dependent properties of IL [emim][Ac] which are used in this study are composed of specific heat capacity, liquid vapor pressure, liquid density, liquid viscosity, and liquid surface tension. The equations in Aspen Plus that represent these properties are CPIGDP, PLXANT, DNLDIP, MULDIP, and SIGDIP. The details of the properties regression are discussed in the following:

4.3.2.1 Specific Heat Capacity

For the specific heat capacity of IL [emim][Ac], the Joback method is used to estimate specific heat capacity of ionic liquid [emim][Ac]; due to this property is not available in the literature. The Joback method uses a four parameter polynomial to describe the temperature dependency of the ideal gas heat capacity as shown in Equation 4.2. These parameters are valid from 273 K to approximately 1000 K. Table 4.6 shows the estimated specific heat capacity of IL [emim][Ac] in the temperature range from 273.15 to 368.15 K.

$$C_p = \sum_{ai} - 37.93 + [\sum_{bi} + 0.21]T + [\sum_{ci} - 3.91.10\text{-}4]T^2 + [\sum_{di} + 2.06.10\text{-}7]T^3 \quad (4.2)$$

Table 4.6 Estimated specific heat capacity of ionic liquid [emim][Ac] at a range of temperature from 273 K to 473 K.

Temperature (K)	Specific heat capacity (J/mol.K)
273	193.64
278	196.20
283	198.75
288	201.30
293	203.85
298	206.39
303	208.93
308	211.47
313	214.01
318	216.54
323	219.07
328	221.59
333	224.11
338	226.63
343	229.14
348	231.65
353	234.15
358	236.65
363	239.15
368	241.63

Next, the data regression mode in Aspen Plus is used. The temperature-dependent correlation parameters of equation CPIGDP, which is the equation that represents specific heat capacity of the substance, are fitted with the estimated data. The correlation equation is shown in Equation 4.3.

$$Cp^{*ig} = C_{1i} + C_{2i}T + C_{3i}T^2 + C_{4i}T^3 + C_{5i}T^4 + C_{6i}T^5 \text{ for } C_{7i} \leq T \leq C_{8i}$$
$$Cp^{*ig} = C_{9i} + C_{10i}T^{C11i} \text{ for } T \leq C_{7i} \quad (4.3)$$

C_1 to C_9 in Equation 4.3 are temperature dependent-correlation parameters for the CPIGDP model. In this study, these parameters are fitted with the estimated specific heat capacity of IL [emim][Ac] in the temperature range from 293 to 318 K, which is the temperature range that was operated in this simulation work. The values of these parameters are shown in Table 4.7.

Table 4.7 Temperature-dependent correlation parameters of specific heat capacity of ionic liquid [emim][Ac] from regression

Parameter/ Name	Symbol	Value (K; J/kmol.K)
CPIG/1	C1i	42972.16
CPIG/2	C2i	584.7068
CPIG/3	C3i	-0.12138
CPIG/4	C4i	0
CPIG/5	C5i	0
CPIG/6	C6i	0
CPIG/7	C7i	0
CPIG/8	C8i	1000
CPIG/9	C9i	0
CPIG/10	C10i	0
CPIG/11	C11i	0

To ascertain the accuracy of these parameters, the regressioned parameters must be checked by using these parameters to calculate back the specific heat capacity of [emim][Ac] and then compare it with the estimated data. From the results, theses regressioned parameter give the consistency result with the estimated

data; and with the correlation coefficient (R^2) equals 0.999. The consistency of regressioned and estimated values is shown in Figure 4.4.

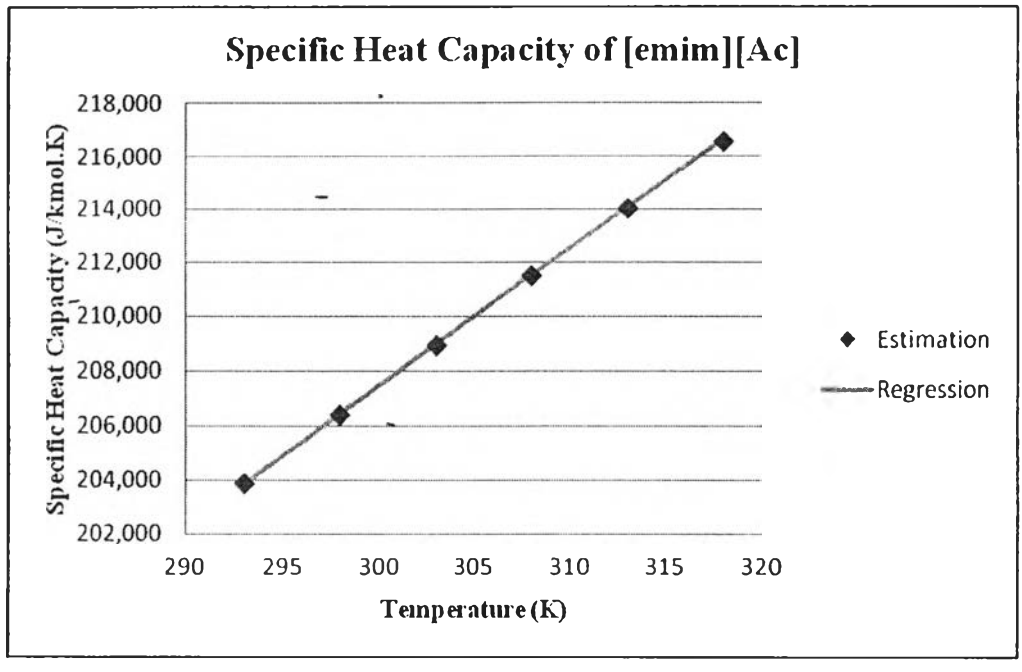

Figure 4.4 The consistency of specific heat capacity between the estimation and regression data of ionic liquid [emim][Ac]

4.3.2.2 Liquid Vapor Pressure

Since ILs are considered substance with zero vapor pressure (negligible vapor pressure), the experimental vapor pressure measurements of ILs are difficult, and the vapor pressure data of ILs are rare. To overcome this problem, the concept of Rudkin (1961) is applied to estimate the vapor pressure of IL [emim][Ac]. Rudkin, considered water as reference fluid and used the Antoine equation (Log P^s = A-B/[T+C]) to relate the vapor pressure P^s of any fluid with the temperature T. Rudkin used a value C = 43 (with T in Kelvin), value corresponding to water, the reference fluid. The equation is shown in Equation 4.4.

$$\log P_s = A - \frac{B}{T - 43} \qquad (4.4)$$

The constant A and B are the function of boiling temperature (T_b), critical temperature (T_c), and critical pressure (P_c) as shown in Equation 4.5 and 4.6. The estimated vapor pressure of IL [emim][Ac] in the temperature range from 273.15 to 523.15 K is shown in Table 4.8.

$$A = \log (P_c)^*(T_c - 43)/(T_c - T_b) \quad (4.5)$$

$$B = \log (P_c)^*(T_c - 43)/(T_b - 43)/(T_c - T_b) \quad (4.6)$$

Table 4.8 The estimated liquid vapor pressure of IL [emim][Ac] in the temperature range from 273.15 to 523.15 K

Temperature (K)	Pressure (Pa)	Temperature (K)	Pressure (Pa)
273.15	6.73248E-07	403.15	0.006218116
283.15	1.93035E-06	413.15	0.009623285
293.15	5.0877E-06	423.15	0.014554907
303.15	1.24466E-05	433.15	0.021551843
313.15	2.8498E-05	443.15	0.031292397
323.15	6.15028E-05	453.15	0.044616543
333.15	0.000125877	463.15	0.062548886
343.15	0.000245626	473.15	0.086321954
353.15	0.00045907	483.15	0.117399418
363.15	0.000825118	493.15	0.157498813
373.15	0.00143129	503.15	0.208613359
383.15	0.002403667	513.15	0.273032506
393.15	0.003918871	523.15	0.353360857

Next, the Data regression mode in the Aspen Plus is used. The temperature-dependent correlation parameters of equation PLXANT, which is

the equation that represents liquid vapor pressure of substance; are fitted with the estimated data. The correlation equation is shown in Equation 4.7.

$$\ln p_i^{*l} = C_{1i} + C_{2i} + \frac{C_{4i}T}{T + C_{3i}} + C_{5i}\ln T = C_{6i}T^{C_{7i}} \text{ for } C_{8i} \leq T \leq C_{9i} \quad (4.7)$$

C_1 to C_9 in Equation 4.7 are temperature dependent-correlation parameters for the PLXANT model. In this study, these parameters are fitted with the estimated liquid vapor pressure of IL [emim][Ac] in the temperature range from 273.15 to 523.15 K. The values of these parameters are shown in Table 4.9.

Table 4.9 Temperature-dependent correlation parameters of liquid vapor pressure of ionic liquid [emim][Ac] from regression

Parameter/ Name	Symbol	Value (K; Pa)
PLXANT/1	C1i	5.549195
PLXANT/2	C2i	-5756.1
PLXANT/3	C3i	-43.715
PLXANT/4	C4i	-2.78E-04
PLXANT/5	C5i	0.518242
PLXANT/6	C6i	4.738097
PLXANT/7	C7i	-0.11424
PLXANT/8	C8i	0
PLXANT/9	C9i	1000

From the results, IL [emim][Ac] shows very extremely low vapour pressure (negligible vapour pressure) that is consistence with the nature of ILs mentioned in the literature review section. The regressed parameter give the consistency result with the estimated data, and with the correlation coefficient (R^2)

equals 0.587. The consistency of regressed and estimated values is shown in Figure 4.5.

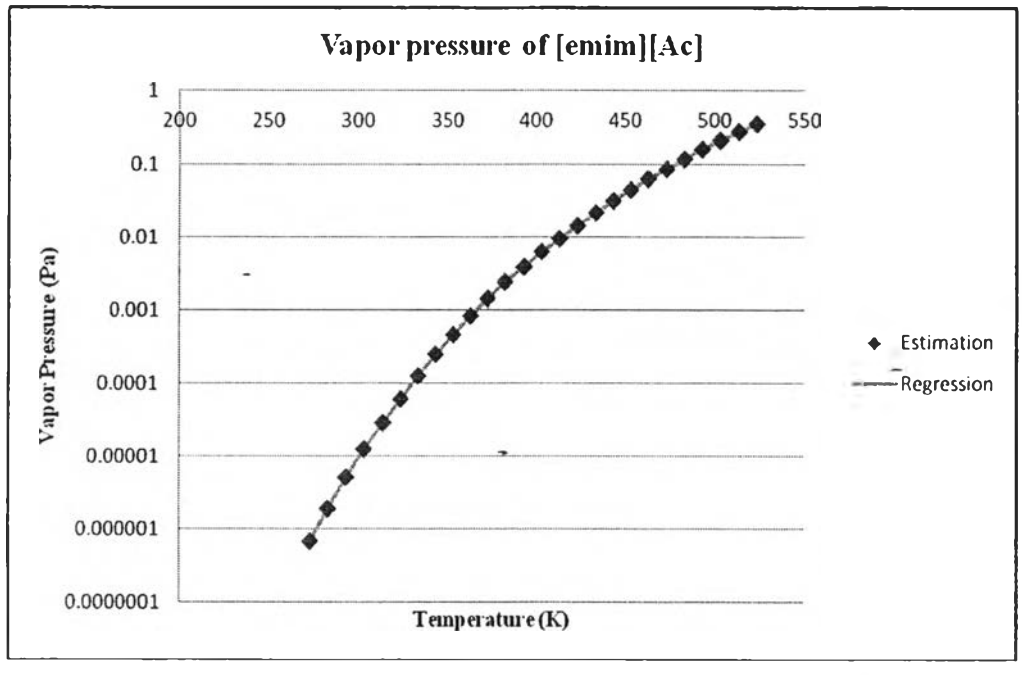

Figure 4.5 The consistency of liquid vapor pressure between the estimation and regression data of ionic liquid [emim][Ac].

4.3.2.3 Liquid Density

The experimental liquid density of IL [emim][Ac] is brought from the study of Hugo *et al.* (2012). The temperature-dependent correlation parameters of equation DNLDIP, which is the equation that represents liquid density of substance, are regressed and fitted with the experimental data. The correlation equation is shown in Equation 4.8.

$$\rho_i^{*l} = C_{1i}/C_{2i}^{(1+(1-T/C3i)C4i)} \text{ for } C_{6i} \leq T \leq C_{7i} \qquad (4.8)$$

C_1 to C_7 in Equation 4.8 are temperature dependent-correlation parameters for the DNLDIP model. In this study, these parameters are fitted with the

experimental liquid density of IL [emim][Ac] in the temperature range from 283.15 to 363.15 K. The values of these parameters are shown in Table 4.10.

Table 4.10 Temperature-dependent correlation parameters of liquid density of ionic liquid [emim][Ac] from regression

Parameter/ Name	Symbol	Value (K; kmol/cum)
DNLDIP/1	C1i	0.37252
DNLDIP/2	C2i	0.220678
DNLDIP/3	C3i	1110.037
DNLDIP/4	C4i	0.528581
DNLDIP/5	C5i	0
DNLDIP/6	C6i	0
DNLDIP/7	C7i	1000

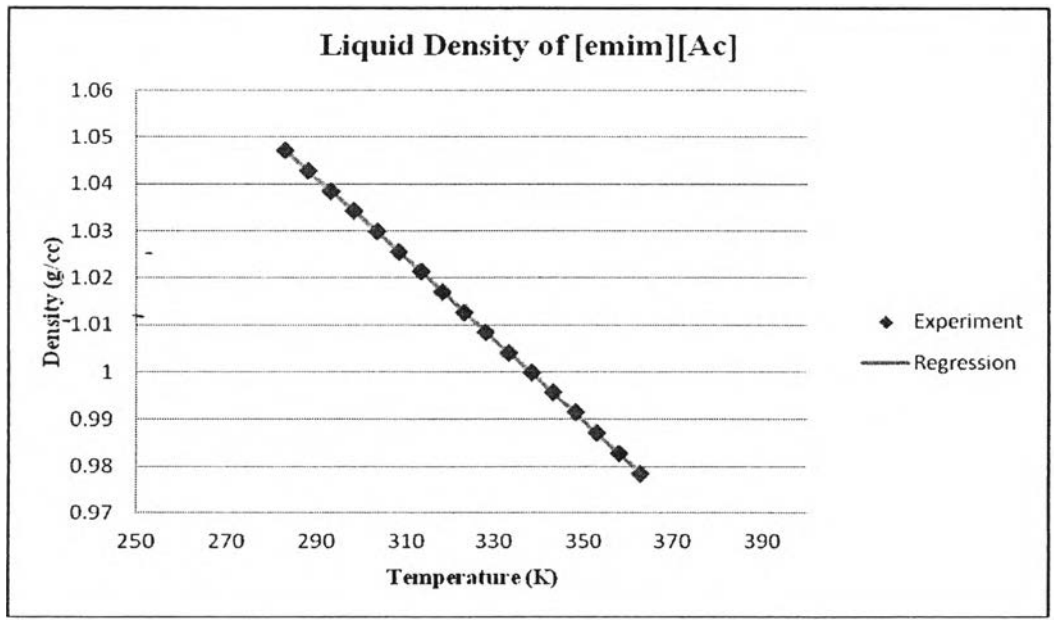

Figure 4.6 The consistency of liquid density between the experiment and regression data of ionic liquid [emim][Ac].

The regressioned parameter give the consistency result with the experimental data, and with the correlation coefficient (R^2) equals 0.999. The consistency of regressioned and estimated values is shown in Figure 4.6.

4.3.2.4 Liquid Viscosity

The experimental liquid viscosity of IL [emim][Ac] is brought from the study of Hugo *et al.* (2012). The temperature-dependent correlation parameters of equation MULDIP, which is the equation that represents liquid viscosity of substance; are regressed and fitted with the experimental data.

$$\ln \eta_i^{*,l} = C_{1i} + C_{2i}/T + C_{3i} \ln T + C_{4i} T^{C5i} \text{ for } C_{6i} \leq T \leq C_{7i} \quad (4.9)$$

C_1 to C_7 in Equation 4.9 are temperature dependent-correlation parameters for the MULDIP model. In this study, these parameters are fitted with the experimental liquid viscosity of IL [emim][Ac] in the temperature range from 283.15 to 363.15 K. The values of these parameters are shown in Table 4.11.

Table 4.11 Temperature-dependent correlation parameters of liquid viscosity of ionic liquid [emim][Ac] from regression

Parameter/ Name	**Symbol**	**Value (K; N-sec/sqm)**
MULDIP/1	C1i	-321.912
MULDIP/2	C2i	20301.95
MULDIP/3	C3i	46.42677
MULDIP/4	C4i	-7.05354
MULDIP/5	C5i	-0.06058
MULDIP/6	C6i	0
MULDIP/7	C7i	1000

The regressed parameter give the consistency result with the experimental data, and with the correlation coefficient (R^2) equals 0.634. The consistency of regressioned and estimated values is shown in Figure 4.7.

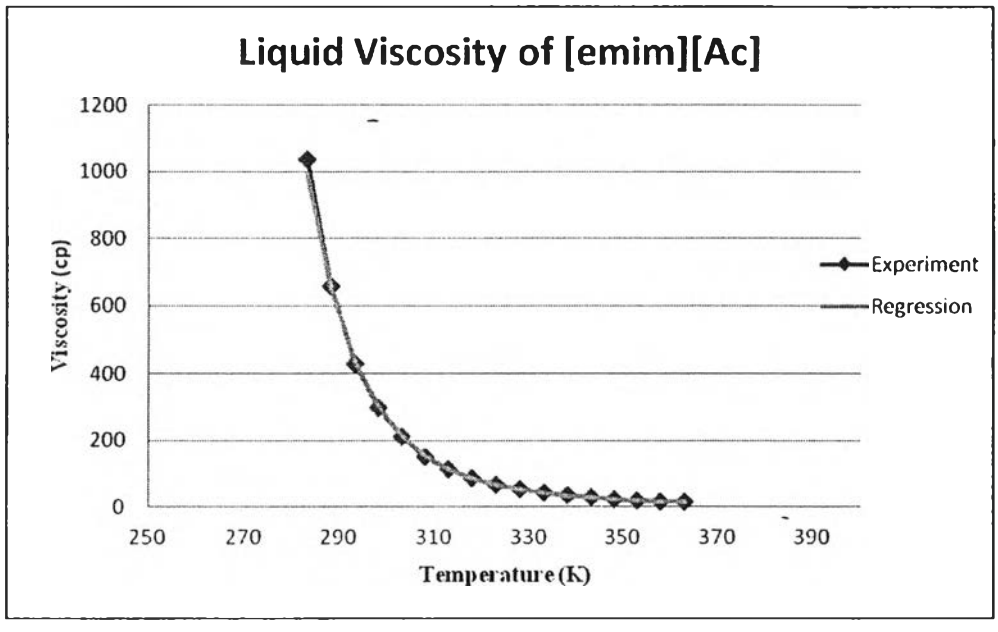

Figure 4.7 The consistency of liquid viscosity between the experiment and regression data of ionic liquid [emim][Ac].

4.3.2.5 Liquid Surface Tension

The experimental liquid surface tension of IL [emim][Ac] is brought from the study of Hugo *et al.* (2012). The temperature-dependent correlation parameters of equation SIGDIP, which is the equation that represents liquid surface tension of substance; are fitted with the experimental data. The correlation equation is shown in Equation 4.10.

$$\sigma_i^{*,l} = C_{1i}(1 - T_{ri})(C_{2i} + C_{3i}T_{ri} + C_{4i}T^2_{ri} + C_{5i}T^3_{ri}) \text{ for } C_{6i} \leq T \leq C_{7i} \quad (4.10)$$

C_1 to C_7 in Equation 4.10 are temperature dependent-correlation parameters for the MULDIP model. T_r is reduced temperature, which is temperature over critical temperature of IL. In this study, these parameters are fitted

with the experimental liquid surface tension of IL [emim][Ac] in the temperature range from 298.1 to 344.2 K. The values of these parameters are shown in Table 4.12.

Table 4.12 Temperature-dependent correlation parameters of liquid surface tension of ionic liquid [emim][Ac] from regression

Parameter/ Name	Symbol	Value (K; N/m)
SIGDIP/1	C1i	0.027268
SIGDIP/2	C2i	-2.89365
SIGDIP/3	C3i	5.889673
SIGDIP/4	C4i	0
SIGDIP/5	C5i	0
SIGDIP/6	C6i	0
SIGDIP/7	C7i	1000

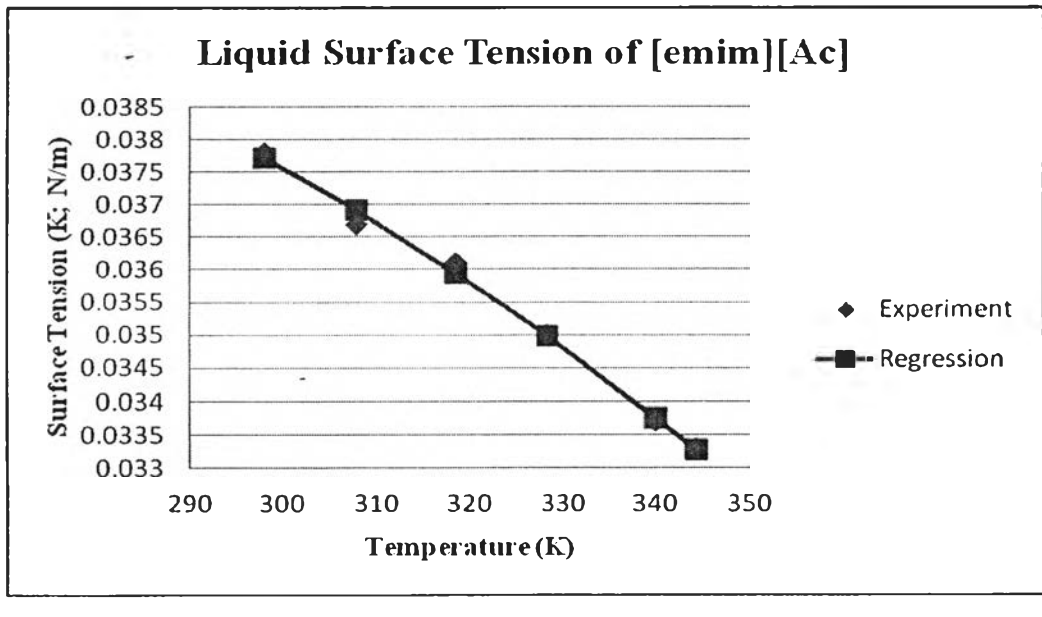

Figure 4.8 The consistency of liquid surface tension between the experiment and regression data of ionic liquid [emim][Ac].

The regressioned parameter give the consistency result with the experimental data; and with the correlation coefficient (R^2) equals 0.997. The consistency of regressioned and estimated values is shown in Figure 4.8.

4.3.3 Thermodynamic Model (Binary Interaction Parameter)

The IL-based system involves the mixture system, which is composed of the solubility of gases in IL (N_2 and CO_2 in [emim][Ac]) and solubility of liquid in liquid ([emim][Ac] in water). The binary interaction parameters of Non-Random Two Liquid (NRTL) are used to calculate the activity coefficient of each substance in the binary system ([emim][Ac] + water). The standard Peng-Robinson (PR-EoS), the Redlich-Kwong-Aspen (RK ASPEN-EoS), and the Henry's constant model is used to calculate the solubility of N_2 and CO_2 in IL [emim][Ac]. Binary interaction parameters of the thermodynamic models in this study are taken from the regression of the experimental data (P-x diagram) reported in the literature.

Many thermodynamic models have been proposed for modeling the phase behavior of ionic liquid + CO_2 systems. In this study, three thermodynamic models available in the Aspen Plus process simulator have been correlated with the experimental data. Then, the results of these three models are compared to find the best one, which has the highest consistency between correlated and experimental data. The experimental CO_2 solubility data is correlated using the two well-known equation of state, the standard Peng-Robinson (PR-EoS) and the Redlich-Kwong-Aspen (RK ASPEN-EoS); and one Henry's constant model.

4.3.3.1 The Standard Peng-Robinson (PR-EoS)

In case of the correlation with the standard PR-EoS, the model parameters, kij(1), kij(2), kij(3) and binary interaction parameter (kij) from 298.1 to 348.2 K of CO_2 + [emim][Ac] system are given in Table 4.13. Parameter kij is fitted to the binary system as a function of temperature with minimized standard deviation. The calculated results from the standard PR-EoS is illustrated in Figure 4.9 along with the experimental data for the binary system CO_2 + [emim][Ac].

Table 4.13 Binary interaction parameters of the standard PR-EoS for the ionic liquid [emim][Ac] (1) + CO_2 (2)

Parameter/ Name	Symbol	Value (SI-unit/K)
PRKBV/1	kij(1)	-74.9236
PRKBV/2	kij(2)	0.137299
PRKBV/3	kij(3)	10000
PRKBV/4	Tlower	1.26E-08
PRKBV/5	Tuppper	1000
Binary interaction parameter	Kij = kij(1) + kij(2)T + kij(3)/T (Equation 2.15)	
	Kij = -74.9236 + (0.137299 x T(K)) + (10000/T(K))	

Table 4.14 Average absolute deviation (AAD %) between experimental and estimated values of mol fraction by the standard PR-EoS for the ionic liquid [emim][Ac] + CO_2

Temperature (K)	Binary interaction parameter values (Kij)	AAD (%)
298.1	-0.44913	0.177253
323.1	0.387714	0.239417
348.2	1.602867	0.213991
	Average AAD (%)	0.210021

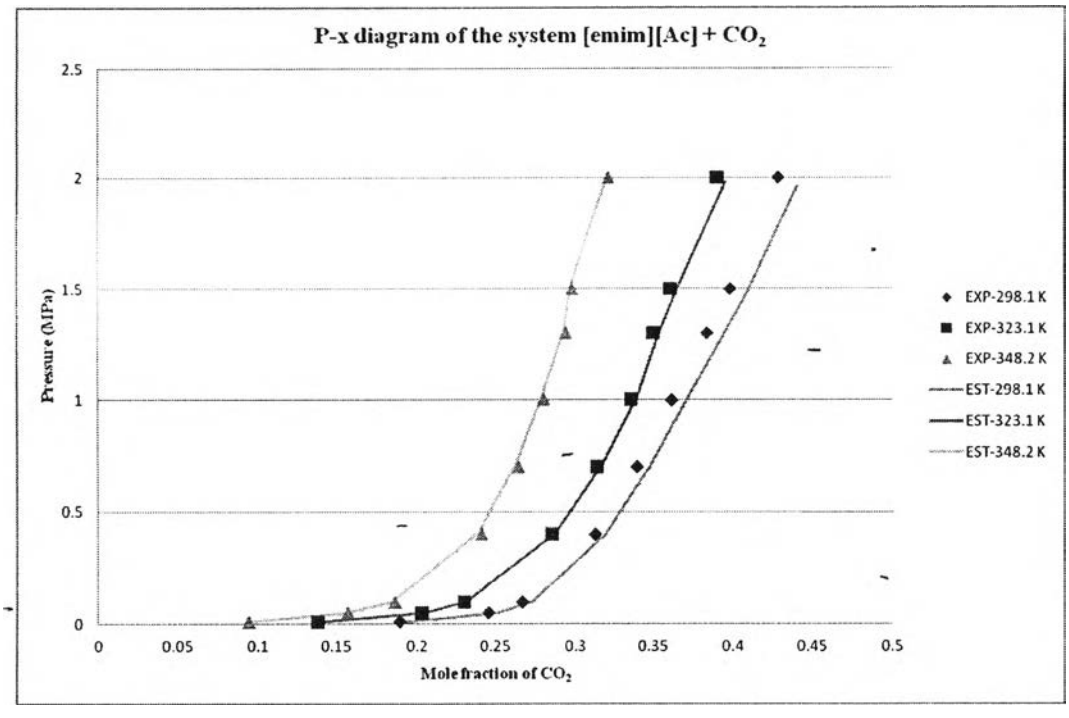

Figure 4.9 P-x diagram of the system CO_2 and ionic liquid [emim][Ac] at three isotherm; 298.2, 323.2, and 348.2 K. Symbols represent the experimental data. Lines represent the estimations by the standard PR-EoS.

Deviation between the experiment and correlated mol fraction are shown in Table 4.14. The AADs are calculated in percent at each isothermal temperature. The AADs at temperature 298.1, 323.1, and 348.2 are 0.177 %, 0.239 %, and 0.214 %, respectively. The average value of AADs is 0.21 %. The standard PR-EoS correlates the data in agreement with the experimental data (average AAD less than 2.0 %). It can be concluded that the use of the standard PR-EoS is acceptable for modeling the solubility of CO_2 in [emim][Ac] over a range of pressure up to 20 bar.

4.3.3.2 The Redlich-Kwong-Aspen (RK ASPEN-EoS)

In this equation of state, quadratic mixing rules which are based on the two-interaction parameters $k_{a,ij}$ and $k_{b,ij}$ are applied. The mixing rules are adequate for mixtures containing polar components that are highly asymmetric with respect to size. The SRK with quadratic mixing rules can describe the experimental data of the solubility of CO_2 in [emim][Ac].

Table 4.15 Binary interaction parameters of the standard PR-EoS for the ionic liquid [emim][Ac] (1) + CO_2 (2)

Parameter/ Name	Symbol	Value (SI-unit/K)
RKAKA0	ka,ij0	-25.6437
RKAKA1	ka,ij1	47.4795
RKAKB0	kb,ij0	-9.60394
RKAKB1	kb,ij1	18.19093
Binary interaction parameter	ka,ij = ka,ij0 + (ka,ij1*T(K)/1000) kb,ij = kb,ij0 + (kb,ij1*T(K)/1000)	
	ka,ij = -25.6437 + (47.4795*T(K)/1000) kb,ij = -9.60394 + (18.19093*T(K)/1000)	

The two binary interaction parameters ($k_{a,ij}$ and $k_{b,ij}$) in the mixing rules are optimized using the experimental CO_2 solubility data. Table 4.15 summarizes the binary interaction parameter of the SRK with quadratic mixing rules at three different temperatures. Figure 4.10 shows the graphical representation of the modeling result and the experimental solubility for the CO_2 + [emim][Ac] system.

The AADs values at the temperature 298.1, 323.1, and 348.2 are 0.819 %, 3.019 %, and 6.720 %, respectively. The binary interaction of the SRK-EoS at high temperature does not seem to be the norm – the higher the temperature, the more deviation from the norm. The average value of AADs is 3.52 %. The average AAD % for the correlation with the SRK-EoS is higher compared to standard PR-EoS. SRK-EoS cannot consistently estimate the solubility of the CO_2 + [emim][Ac] system with the experimental solubility data; especially at high temperature. In conclusion, the standard PR-EoS predicts better CO_2 solubility for CO_2 + [emim][Ac] system than the standard SRK-EoS.

Table 4.16 Average absolute deviation (AAD %) between experimental and estimated values of mol fraction by the standard SRK-EoS for the ionic liquid [emim][Ac] + CO_2

Temperature (K)	Binary interaction parameter values (Kij)		AAD (%)
	ka,ij	kb,ij	
298.1	-11.4901	-4.18122	0.819231
323.1	-10.3031	-3.72645	3.019835
348.2	-9.11134	-3.26986	6.720232
		Average AAD (%)	3.519766

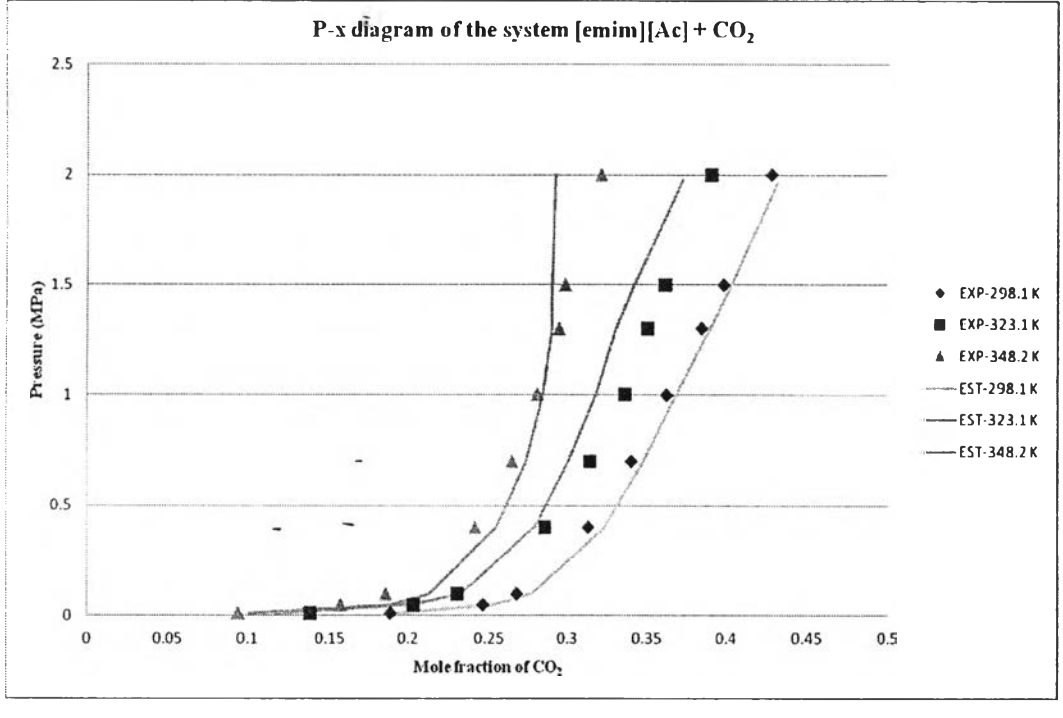

Figure 4.10 P-x diagram of the system CO_2 and ionic liquid [emim][Ac] at three isotherm; 298.2, 323.2, and 348.2 K. Symbols represent the experimental data. Lines represent the estimations by the standard SRK-EoS.

4.3.3.3 Henry's Constant Model

The Henry's constant model is used when Henry's Law is applied to calculate K-values for dissolved gas components in a mixture. Henry's Law is available in all activity coefficient property methods in Aspen Plus. In this study, Henry's constant model in Non-Random Two Liquid (NRTL) model is applied to correlate with the experimental data. The model calculates Henry's constant for a dissolved gas component in the solvent. The general equation of Henry's constant of the Aspen is shown as Equation 4.11:

$$\ln H_i = a_{iA} + b_{iA}/T + c_{iA}\ln T + d_{iA}T + e_{iA}/T^2 \text{ for } T_L \leq T \leq T_H \qquad (4.11)$$

The model parameters "a" to "e" are fitted to the experimental data; these values are shown in Table 4.17.

Table 4.17 Parameters of the Henry's law constant model for the binary system ionic liquid [emim][Ac] + CO_2

Parameter/ Name	Symbol	Value (SI-unit/K)
HENRY/1	aij	-958.843
HENRY/2	bij	-10000
HENRY/3	cij	171.3431
HENRY/4	dij	0
HENRY/5	Tlower	0
HENRY/6	Tupper	2000
HENRY/7	eij	0

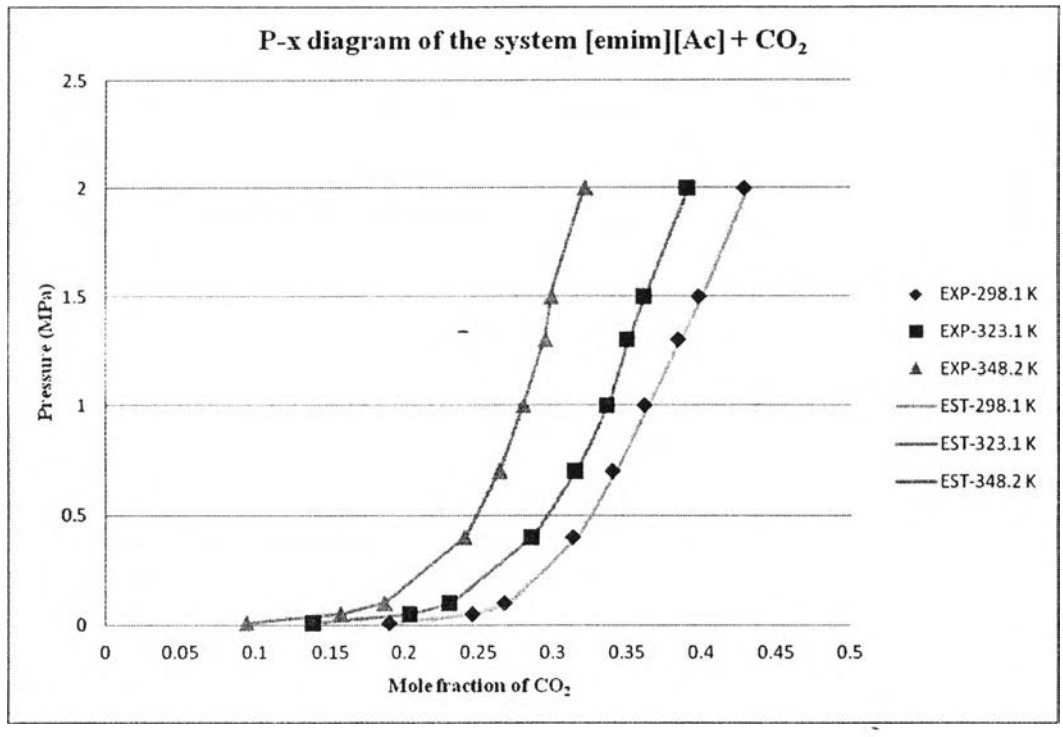

Figure 4.11 P-x diagram of the system N_2 and ionic liquid [emim][Ac]. Symbols represent the experimental data. Lines represent the estimations by Henry's constant model.

The correlated results from the Henry's law model along with the experimental data for the binary system CO_2 + [emim][Ac] are shown in Figure 4.11. The AADs values at the temperature 298.1, 323.1, and 348.2 are 0.264 %, 0.117 %, and 0.087 %, respectively. The average value of AADs is 0.16 %. For all thermodynamic model used in this study, Henry's constant model provides the lowest average AAD for the experimental solubility correlation. As a results, Henry's constant is determined the best model to represent the CO_2 solubility in IL [emim][Ac] at low pressure up to 20 bar and temperature of 298.1, 323.1, and 348.2 K.

Henry's law model is also used to correlate the solubility of N_2 in [emim][Ac] because it is presence in the flue gas composition. The model parameters are shown in Table 4.18. Refers to the study of Shiflett *et al* (2010), the solubility of N_2 in ionic liquid 1-butyl-3-methylimidazolium tetrafluoroborate

[bmim][Bf4] is used instead of [emim][Ac] because the solubility of N_2 in [emim][Ac] have not been reported in any literature. In this study, the N_2 solubility is taken from the study of johan *et al.* (2006).

Table 4.18 Parameters of the Henry's constant model for the binary system ionic liquid [emim][Ac] + N_2

Parameter/ Name	Symbol	Value (SI-unit/K)
HENRY/1	aij	-212.899
HENRY/2	bij	9377.806
HENRY/3	cij	33.61916
HENRY/4	dij	0
HENRY/5	Tlower	0
HENRY/6	Tupper	2000
HENRY/7	eij	0

The calculated results from the Henry's law model are illustrated in Figure 4.12 along with the experimental data for the binary system CO_2 + N_2. The AAD of this system is 0.311 %.

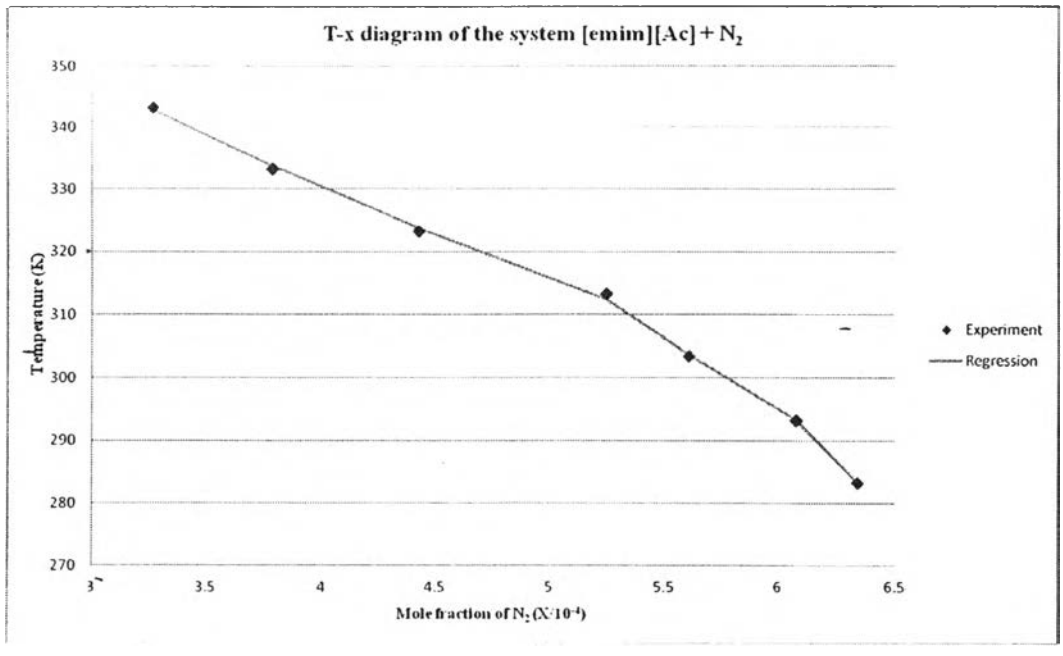

Figure 4.12 T-x diagram of the system N_2 and ionic liquid [emim][Ac]. Symbols represent the experimental data. Lines represent the estimations by the Henry's constant model.

4.3.3.4 The Non-Random Two Liquid (NRTL)

Apart from the gases solubility in ionic liquid, liquid solubility in ionic liquid is also considered because of existing water in the system. In this study, the well-known NRTL activity coefficient model is used to correlate the solubility of water in [emim][Ac]. Table 4.19 shows the binary interaction parameters adjusted to the experiment solubility data of water in [emim][Ac], which are $(g_{12}-g_{22})/R$ and $(g_{21}-g_{11})/R$. Both binary parameters are related to τ_{12} and τ_{21}, respectively. In this work, the parameter α is assumed to be constant value of 0.338354 in order to obtain the accurate results (Al-Rashed *et al.*, 2012). The P-x diagram of [emim][Ac] + water mixture at 7 temperatures (293.15, 303.15, 313.15, 323.15, 333.15, 343.15, and 353.15 K) are depicted in Figure 4.13. The solubility of water in [emim][Ac] are taken from the study of Christian *et al.* (2012).

Table 4.19 Binary interaction parameters of the NRTL for the ionic liquid [emim][Ac] + H_2O system

Parameter/ Name	**Symbol**	**Value (SI-Unit/ K)**
NRTL/1	Aij	80
NRTL/1	Aji	9.789126
NRTL/2	Bij	10000
NRTL/2	Bji	-3521.07
NRTL/3	Cij	0.338354
NRTL/4	Dij	0
NRTL/5	Eij	0
NRTL/5	Eji	0
NRTL/6	Fij	0
NRTL/6	Fij	0
Binary interaction parameter	$\tau_{12} = (g_{12}-g_{22})/RT$ $\tau_{21} = (g_{21}-g_{11})/RT$	
	(g12-g21)/R = [80 x T(K)] + 10000 (g21-g12)/R = [9.789126 x T(K)] – 3521.02	

The correlated pressures obtained from the NRTL are in good agreement with the experimental equilibrium pressures. The AADs of the estimation and regression are shown in Table 4.20. The average AAD of this binary system is 0.75 %.

Table 4.20 Average absolute deviation (AAD %) between experimental and estimated values of pressure by the NRTL for the [emim][Ac] + H_2O system

Temperature (K)	Binary interaction parameter values (Kij)			AAD (%)
	$(g_{12}-g_{22})/R$	$(g_{21}-g_{11})/R$	α	
293.15	33452	-651.391	0.338354	0.499528
303.15	34252	-553.500	0.338354	0.293275
313.15	35052	-455.608	0.338354	0.213706
323.15	35852	-357.717	0.338354	0.498887
333.15	36652	-259.826	0.338354	0.888916
343.15	37452	-161.935	0.338354	1.246699
353.15	38252	-64.0434	0.338354	1.574436
			Average AAD (%)	0.745064

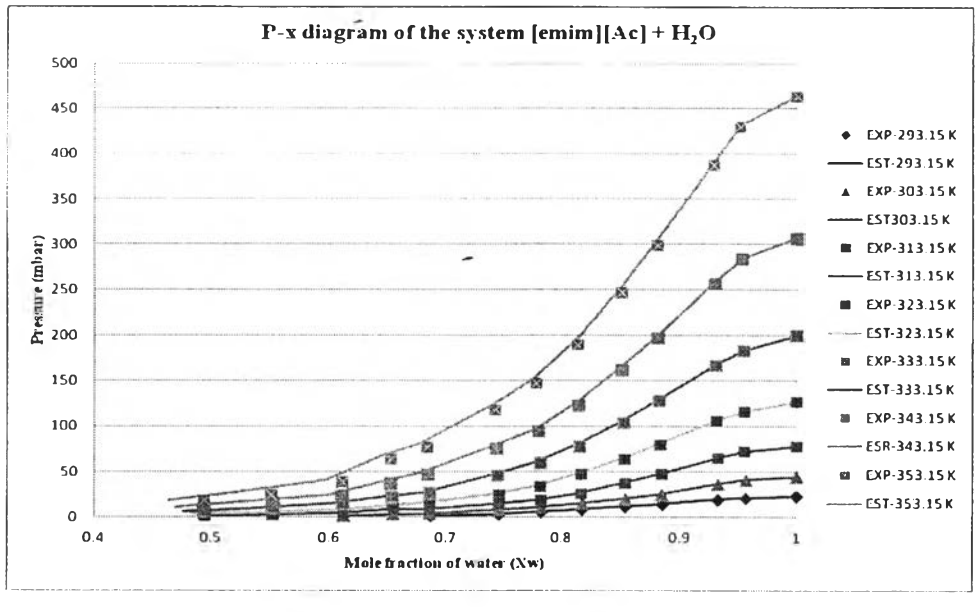

Figure 4.13 P-x diagram of the system H_2O and ionic liquid [emim][Ac] at seven isotherm; 293.15, 303.15, 313.15, 323.15, 333.15, 343.15, and 353.15 K. Symbols represent the experimental data. Lines represent the estimations by the NRTL.

4.3.4 Equilibrium Model

In this study, IL ([emim][Ac]) shows chemical absorption behavior which differs from other ILs, the reaction calculation mode in Aspen Plus is therefore required. Many researches on reaction mechanism of [emim][Ac] have been done, but real reaction mechanism has not been confirmed. Therefore, this study is based on the possible reaction paths as shown in Figures 4.14 and 4.15.

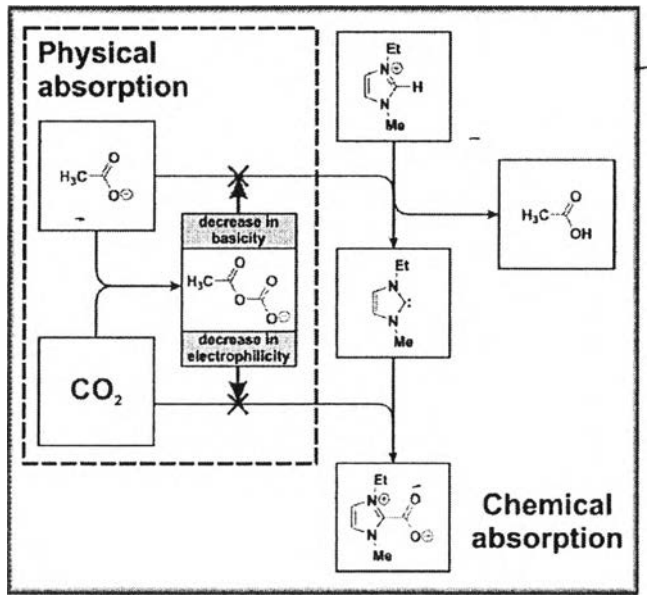

Figure 4.14 Possible reaction paths leading to either physical or chemical absorptions of ionic liquid [emim][Ac] (Holloczki *et al.*, 2013).

IL [emim][Ac] consists of imidazolium cation and acetate anion. The chemical reaction of [emim][Ac] occurred via proton transfer process. Hydrogen atom at C2 position on the imidazolium cation is transferred and forms the ion pair with [emim][Ac] ([C2C1Im][HOAc]), such molecule called "carbene" is shown in step 2 on Figure 4.15. Then, carbene molecule donates the electron pair to carbon dioxide molecule, causing the acetate-hydrogen anion to be eliminated from the carbene molecule and forms the acetic acid. This reaction is a reversible process.

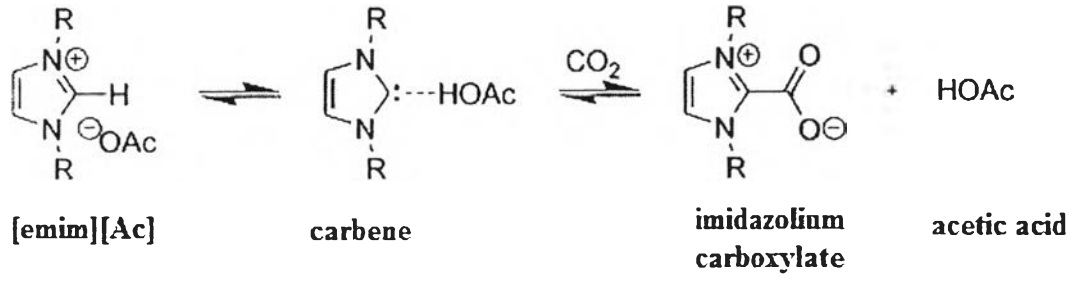

Figure 4.15 Formation of imidazolium carboxylate and acetic acid.

In the literature, carbon dioxide solubility in ionic liquid [emim][Ac] show extremely unusual phase behavior, (CO_2) dissolves in the ionic liquid at a large concentration (up to about 20 mol % of CO_2 with almost no vapor pressure above the mixture). Such behavior of [emim][Ac] is similar to [bmim][Ac] and [eemim][Ac]. In all three cases, CO_2 forms molecular complexes (or chemical compounds) with ionic liquid. NMR spectroscopy has identified the structure imidazoilum-2-carboxylate as shown in step 3 of Figure 4.15. Shiflett and *et al.* (2010) proposed the equilibrium calculation based on their experiment measurement (CO_2 + [bmim][Ac]) as shown in Figure 4.16. Due to the similarity of CO_2 absorption behaviors between [bmim][Ac], [emim][Ac] ,and [eemim][Ac]. The equilibrium calculation of [emim][Ac] is assumed equivalent to [bmim][Ac] because there is no reported experiment for [emim][Ac].

Rxn1: $emimAc + CO_2 \leftrightarrow emimCO_2$

Rxn2: $emimCO_2 + emimAc \leftrightarrow emim_2CO_2$

Rxn3: $emim_2CO_2 + emimAc \leftrightarrow emim_3CO_2$

Figure 4.16 The reactions of [emim][Ac] with CO_2.

The reaction of [emim][Ac] and CO_2 consists of three minor reactions. One molecule of [emim][Ac] reacts with one molecule of CO_2 and form the imidazolium carboxylate. Then, the imidazolium carboxylate continues to react with another molecules of [emim][Ac] and forms the new imidazolium carboxylate,

which consist of two moles of [emim][Ac] in the molecule. This molecule continues to react with another molecule of [emim][Ac], and finally the imidazolium carboxylate with three moles of [emim][Ac] is formed.

In this study, equilibrium constant reaction model is employed to calculate the reaction of [emim][Ac] in the simulation. The Aspen Physical Property System can calculate these equilibrium constants from the correlations (as a function of temperature) as shown in Equation 4.12.

$$\ln K_{eq} = A + B/T + C \ln T + DT, \; T \text{ in Kelvin} \qquad (4.12)$$

A, B, C, and D are adjustable constant parameters for the equilibrium constants. These parameters are correlated to the composition measurement of the reaction at equilibrium condition. The equilibrium constants of all reactions at temperature of 273.15 to 368.15, and equilibrium constant parameters are shown in Table 4.21. Equilibrium constant in this study is defined as mole fraction of products over mole fraction of reactants, shown in Figure 4.17. The "REAC-DIST" type equilibrium model is used for reaction calculation in the absorber, while the "POWER LAW" is used for RCSTR/FLASH unit.

Rxn1: $K_{eq} = [emimCO_2]/[emimAc]*[CO_2]$

Rxn2: $K_{eq} = [emim_2CO_2]/[emimAc]*[emimCO_2]$

Rxn3: $K_{eq} = [emim_3CO_2]/[emimAc]*[emim_2CO_2]$

Figure 4.17 Equilibrium constant of the reactions of [emim][Ac] with CO_2.

Based on all of these parameters (pure component properties, critical properties, thermodynamic models for gas and liquid solubility, and reaction model) a process simulation of IL [emim][Ac] can be carried out to meet the same target as MEA-based process.

Table 4.21 Equilibrium constants at a range of temperature from 273.2 to 368.2 K; and equilibrium constant parameters for the reaction of CO_2 + [emim][Ac] system

Temperature (K)	Equilibrium constant (K_{eq})		
	Reaction 1	**Reaction 2**	**Reaction 3**
273.15	32.45636	1.698461	3.406466
278.15	27.09424	1.930073	3.289424
283.15	22.7627	2.18339	3.180329
288.15	19.23961	2.459405	3.078453
293.15	16.35534	2.759086	2.983152
298.15	13.97941	3.08337	2.893851
303.15	12.01066	3.43316	2.81004
308.15	10.37013	3.809324	2.73126
313.15	8.99577	4.212694	2.6571
318.15	7.838505	4.644062	2.587191
323.15	6.859285	5.104179	2.521201
328.15	6.026852	5.593756	2.458829
333.15	5.316047	6.113461	2.399804
338.15	4.706508	6.66392	2.34388
343.15	4.181674	7.245715	2.290832
348.15	3.728004	7.859385	2.240458
353.15	3.334378	8.505427	2.192571
358.15	2.99162	9.184294	2.147003
363.15	2.692125	9.896396	2.103598
368.15	2.429564	10.6421	2.062214
Equilibrium constant parameters			
	Reaction 1	**Reaction 2**	**Reaction 3**
A	-6.5655	7.6412	-0.7193
B	2743.9	-1942.5	531.27
C	-	-	-
D	-	-	-

4.4 IL-based CO_2 Capture Process

4.4.1 Process Description

The IL-based CO_2 capture process is designed to achieve the same specifications as the MEA process. The flow diagram of IL process is shown in Figure 4.18. The plant is similar to the one used by Shiflett *et al.* (2010). Even the IL [emim][Ac] shows chemical absorption behaviour and has very high CO_2 capture capacity compared to most of ILs, but [emim][Ac] has lower capacity when compared to MEA. To improve the solubility of CO_2 in [emim][Ac], the scrubber system are operated under high pressure and low temperature. In this study, the absorber is operated under pressure at 618 kPa. The absorber pressure and IL flow rate are optimized to minimize the energy consumption and meet the same target as MEA process. From the process flow diagram, CO_2 is chemically absorbed by [emim][Ac] to get the same composition of CO_2 in the vent gas compare to MEA process. Rich IL solvent is heated up before entering the regeneration unit. Regeneration process is different from MEA by using flash technique instead of stripper column (Aspen Plus RCSTR). IL-rich solution is regenerated by decreasing the pressure to the atmospheric pressure and increasing temperature to about 80 ^{o}C, which is the temperature that CO_2 is stripped off completely. IL-lean solution is pumped back and cooled down to -2 ^{o}C by using refrigeration system. Dichlorodifluoromethane is selected as the refrigerant by considering of its normal boiling point and outlet temperature of cooled stream. Solvent after exiting the refrigeration is recycled back to the top of the absorber. The simulation specifications of IL process are shown in Table 4.23.

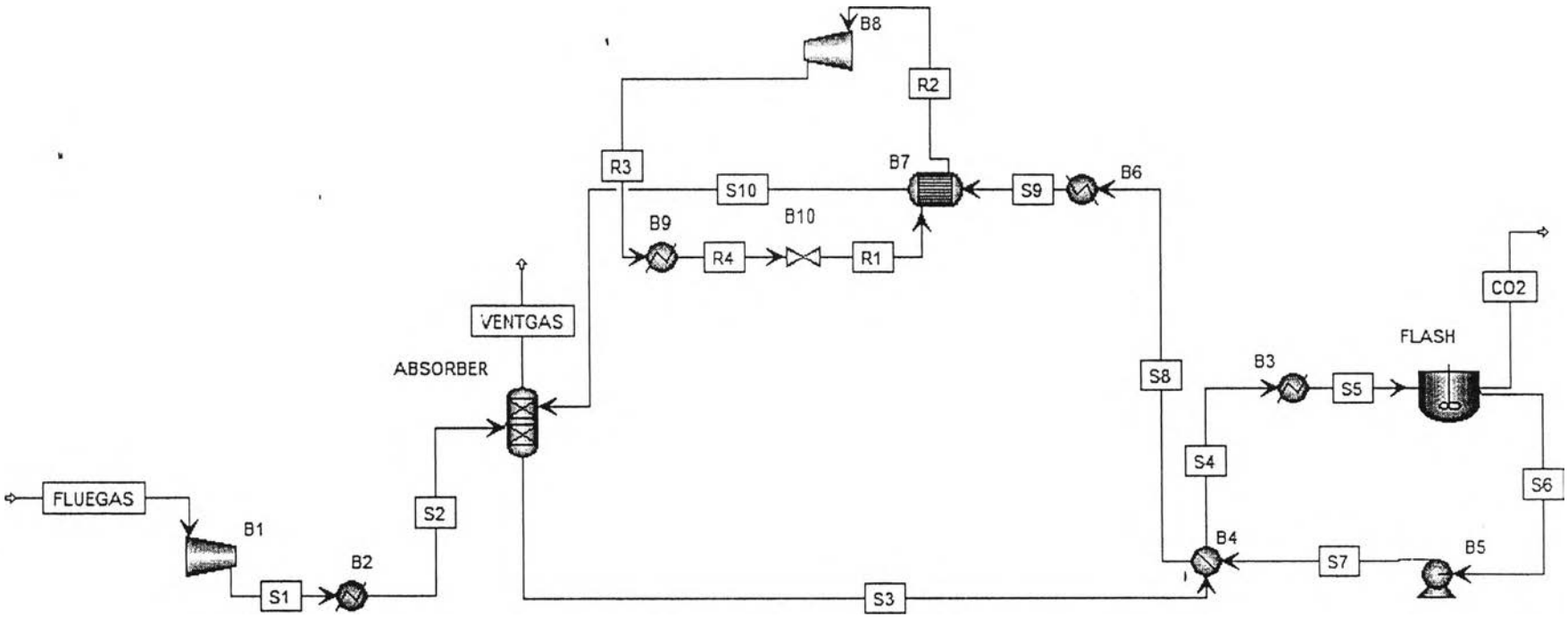

Figure 4.18 IL-based CO_2 capture flow diagram by Aspen Plus simulation.

Table 4.22a Stream summary of IL-based CO_2 capture process

Stream	CO2	FLUEGAS	R1	R2	R3	R4
Temperature (^{O}C)	80.8	142	-30.4	-30.4	51	16
Pressure (bar)	1.013	1.013	0.989	0.989	5.79	5.79
Vapor Fraction	1	1	0.252	1	1	0
Mole Flow (kmol/hr)	133.226	1013.526	851.52	851.52	851.52	851.52
Mass Flow (kg/hr)	5836.315	30732.01	102960	102960	102960	102960
Volume Flow (cum/hr)	3856.934	34532.38	4284.18	16791.4	3594.016	72.52
Enthalpy (Gcal/hr)	-12.313	-12.877	-103.843	-100.799	-99.741	-103.843
Mole Flow (kmol/hr)						
N2	1.446	867.266	0	0	0	0
O2	0	0	0	0	0	0
CO	0	0	0	0	0	0
CO2	131.634	146.26	0	0	0	0
CH4	0	0	0	0	0	0
H2O	0.146	0	0	0	0	0
BMIMAC	0	0	0	0	0	0
BMIMCO2	0	0	0	0	0	0
BMIM2CO2	0	0	0	0	0	0
BMIM3CO2	0	867.266	0	0	0	0
DICHL-01	0	0	851.52	851.52	851.52	851.52

Table 4.22b Stream summary of IL-based CO_2 capture process

Stream	S1	S2	S3	S4	S5	S6
Temperature (^{O}C)	540.6	39	-23.3	9.9	58.1	80.8
Pressure (bar)	7.908	7.908	6.18	6.18	6.18	1.013
Vapor Fraction	1	1	0	0	0.001	0
Mole Flow (kmol/hr)	1013.526	1013.526	663.786	663.786	663.786	699.972
Mass Flow (kg/hr)	30732.01	30732.01	178545.2	178545.2	178545.2	172708.8
Volume Flow (cum/hr)	8693.962	3311.62	249.288	250.397	253.478	265.955
Enthalpy (Gcal/hr)	-9.717	-13.663	-153.925	-152.576	-148.612	-136.299
Mole Flow (kmol/hr)						
N2	867.266	867.266	1.448	1.448	1.448	0.002
O2	0	0	0	0	0	0
CO	0	0	0	0	0	0
CO2	146.26	146.26	2.939	2.939	2.939	4.178
CH4	0	0	0	0	0	0
H2O	0	0	0.539	0.539	0.539	0.393
BMIMAC	0	0	347.677	347.677	347.677	517.088
BMIMCO2	0	0	127.66	127.66	127.66	10.116
BMIM2CO2	0	0	58.454	58.454	58.454	64.335
BMIM3CO2	0	0	125.07	125.07	125.07	103.86
DICHL-01	0	0	0	0	0	0

Table 4.22c Stream summary of IL-based CO_2 capture process

Stream	S7	S8	S9	S10	VENTGAS
Temperature (^{O}C)	81	50.4	45	-2	7.4
Pressure (bar)	7.908	7.908	7.908	7.908	6.18
Vapor Fraction	0	0	0	0	1
Mole Flow (kmol/hr)	699.972	699.972	699.972	699.972	880.468
Mass Flow (kg/hr)	172708.8	172708.8	172708.8	172708.8	24898.84
Volume Flow (cum/hr)	265.941	265.365	264.896	263.632	3311.969
Enthalpy (Gcal/hr)	-136.243	-137.592	-138.703	-141.748	-1.496
Mole Flow (kmol/hr)					
N2	0.002	0.002	0.002	0.002	865.823
O2	0	0	0	0	0
CO	0	0	0	0	0
CO2	4.178	4.178	4.178	4.178	14.63
CH4	0	0	0	0	0
H2O	0.393	0.393	0.393	0.393	0.014
BMIMAC	517.088	517.088	517.088	517.088	0
BMIMCO2	10.116	10.116	10.116	10.116	0
BMIM2CO2	64.335	64.335	64.335	64.335	0
BMIM3CO2	103.86	103.86	103.86	103.86	0
DICHL-01	0	0	0	0	0

4.4.2 Key Process Simulation Specifications

A summary of simulation inputs are displayed in Table 4.23.

Table 4.23a IL-based CO_2 capture plant key process simulation specifications

FLUEGAS (Post-combustion Flue Gas Stream)	Temperature (°C)	142
	Pressure (kPa)	101.3
	Molar Flow (kmol/hr)	1013.526
	Composition (mole fraction)	
	N_2	0.855692
	CO_2	0.144308
	H_2O	-
B1 (Flue Gas Compressor)	Discharge Pressure (kPa)	791.03
B2 (Flue Gas Cooler)	Outlet Temperature (°C)	39
ABSORBER (Absorber)	Number of Stages	20
	Pressure (kPa)	618.14
	CO2 Removal (%)	90
S10 (Absorbent Inlet Stream)	Temperature (°C)	-2.0
	Pressure (kPa)	790.8
	Molar Flow (kmol/hr)	700.1
	Composition (mole fraction)	
	N2	7.14185E-06
	CO2	0.005926305
	H2O	0.000791317
	BMIMAC	0.738536978
	BMIMCO2	0.014595079
	BMIM2CO2	0.091682748
	BMIM3CO2	0.148460432
	DICHL-01	-

Table 4.23b IL-based CO_2 capture plant key process simulation specifications

B4 (Rich/Lean HEX)	Hot Side Outlet Temperature (°C)	50.4
	Cold Side Outlet Temperature (°C)	9.9
	Temperature Approach (°C)	5
B3 (Flash Pre-heater)	Temperature (°C)	58.1
	Pressure (kPa)	618.14
FLASH (Flash Tank/RCSTR)	Temperature (°C)	81
	Pressure (kPa)	101.3
B5 (Flash Pump)	Outlet Pressure (kPa)	791.03
B6 (Cooler)	Temperature (°C)	45
B7 (Heat Exchanger)	Hot Side Outlet Temperature (°C)	-2
	Cold Side Outlet Temperature (°C)	-30.4
	Temperature Approach (°C)	5
B8 (Compressor)	Discharge Pressure (kPa)	579
B9	Outlet Temperature (°C)	16
B10	Outlet Pressure (kPa)	98.9
***Note**		
Stream	**Vapor Fraction**	
R1	0.252	
R2	1	
R3	1	
R4	0	

4.5 Comparison of MEA and IL-based CO_2 Capture Process

In this study, the MEA-based process separates about 90 % of CO_2 with annual capacity 47,109 tons, and purity of 98.18 %. The operating specifications of both processes are discussed in sections 4.1 and 4.4. The summaries of process specification are shown in Table 4.24. This study is compared to the commercial

MEA-based process with 90 % capture, 47,000 ton of annual capacity, and 95 % of purity. The IL-based process is designed to achieve the same specification as the MEA-based process. The IL-based process separates 47,100 tons/year, which results in a recovery of 90.01 % of CO_2, and a little bit higher purity compared to MEA of 99.26 %. The summaries of scrubbing performances are shown in Table 4.25.

The mass flow rate of MEA and IL-based process are 41.78 and 47.98 kg/s. The operating pressure of MEA-base process is at the pressure near atmospheric pressure, while IL- process is operated at about 6 bars. The higher mass flow rate and operating pressure of IL [emim][Ac] is due to its lower absorption capacity compared to MEA. The compressor and refrigeration system are employed to make the suitable operating condition for IL-based process. According to Shiflett *et al.* (2010), the additional energy and equipments for compressing the flue gas and cooling the absorbent (refrigeration) will be partially offset by the energy and equipments saving in the regeneration process.

The utility requirements for the MEA-based process are steam and electricity. The major utility of this process is steam, which is used for heating up the reboiler and stripper pre-heater. The large amount of duty (steam) is required because of strong chemical interaction between CO_2 and MEA (carbamate formation). Electricity in the MEA-based process is required for pumps. For the IL-based process, the major required duty is electricity that used for compressor and refrigeration, while the duty from steam is less than MEA because [emim][Ac] is reported to have lower heat of absorption compared to MEA. The heat duty and utilities requirement for the MEA and IL-based process are summarized in Table 4.26 to 4.29. The total amount of energy requirement for the IL-based process is 8,710 kW, which is 13.5 % lower compared to MEA-based process.

To ascertain the economic benefit of the IL-base process, the evaluation of the total investment is employed. The percentage of delivered-equipment cost method is used in this study. The cost of delivering equipment is represented as a percentage of the purchased equipment cost. The percentage and total investment cost of MEA and IL-based process are shown in Tables 4.32 and 4.33.

Table 4.24 Process specification of MEA and IL-based process

	MEA			IL		
	T (K)	P (kPa)	m(kg/s)	T (K)	P (kPa)	m(kg/s)
Absorber						
Flue gas	320.0	115.1	9.03	313	790.8	8.54
Vent gas	328.0	101.3	7.63	281	618.0	6.92
Absorbent inlet	309.0	135.8	41.78	272	790.8	47.98
Absorbent outlet	325.0	101.3	43.19	250	618.0	49.6
Stripper/Flash						
CO_2 outlet	302.0	101.3	1.64	354	101.3	1.62
Absorbent inlet	363.0	239.2	43.19	332	618.0	49.6
Absorbent outlet	390.0	173.0	41.55	354	101.3	47.98

Table 4.25 Scrubbing performance and cost of MEA and IL-based process

	MEA	IL
CO2		
Capacity (tons/year)	47,109	47,100
Recovery (%)	90.03	90.01
Purity (%)	98.18	99.26
Utilities		
Steam (kg/s)	5.05	1.85
Cooling water (kg/s)	226.33	150.06
Energy		
Steam (kW)	10,061	3,738
Electricity (kW)	8.57	4,972
Total (kW)	10,069	8,710
Total capital investment (million $)	18,656,329	17,899,587

To estimate the cost, the number of equipment, type of equipment, materials of construction, and size of equipments are needed. Size parameters are calculated and provided by the process simulation program. Type and materials of construction are based on the commercial configuration CO_2 capture plant reported in the literature. The costs of equipments are estimated using an online cost estimator (http://highered.mcgraw-hill.com) and convert all cost to the year 2012 (engineering plant index for the year 2013 -= 576). Size parameters, type of equipment, materials of construction and cost of investment for MEA and IL-based process are shown in Tables 4.30 and 4.31. The additional equipment for IL-based process including compressor and refrigeration system, is not included with the engineered equipment because it could be purchased as a ready to install package (59.31 % of total investment). The raw materials (absorbent cost) are also included in the investment cost due to the high cost of IL, which is approximately 10 times higher than MEA. The MEA and IL initial charge volume of working fluid are 13,992 and 19,907 kg; with the cost of $2.25 and 20 $/kg, respectively. The initial charge volume and cost of working fluid is evaluated based on the study of Shiflett *et al.* (2010). The investment costs of MEA and IL-based process are illustrated in Tables 4.32 and 4.33. IL-based process shows lower capital investment cost by 3.75 % compared to MEA-based process.

For conclusion, this study focuses on the comparison of the energy requirement and capital investment cost between conventional MEA and IL-based process using ionic liquid [emim][Ac] for post-combustion carbon dioxide capture process, based on the flue gas from coal burning power plant 180 MWe. The results show both lower energy requirement and capital investment cost of IL-based compared to MEA by 13.5 % and 3.75 %, respectively. As the results, IL-based process shows its potential to replace conventional MEA-based process. However, further studies on this IL [emim][Ac] are recommended to ascertain this potential.

Table 4.26 Unit energy consumption of MEA-based process

Unit	Duty type	Duty (kW)
Rich Amine Pump	Electricity	8.43
Lean Amine Pump	Electricity	-
Reflux Pump	Electricity	0.14
Stripper Pre-heater	Steam	2,086.12
Reboiler	Steam	7,974.93
Total Energy		**10069.62**

Table 4.27 Unit energy consumption of IL-based process

Unit	Duty type	Duty (kW)
B1(Flue Gas Compressor)	Electricity	3,676.0
B5 (Flash Pump)	Electricity	65.14
B8 (Refrigerator Compressor)	Electricity	1,230.41
FLASH	Steam	3,738.07
Total Energy		**8,709.63**

Table 4.28 Summary of unit utilities consumption of MEA-based process

Unit	Utility type	Volume (kg/s)
Scrubber	Process Water	0.50399
Water Makeup	Process Water	0.23388
Total		**0.73787**
Condenser	Cooling Water	20.332782
Cooler	Cooling Water	206.000862
Total		**226.333644**
Stripper Pre-heater	Steam	1.04671079
Re-boiler	Steam	4.00143096
Total		**5.04814175**

Table 4.29 Summary of unit utilities consumption of IL-based process

Unit	Utility type	Volume (kg/s)
B2 (Flue Gas Chiller)	Cooling Water	137.477366
B6 (Cooler)	Cooling Water	12.5854935
Total		**150.0628595**
FLASH (Flash Tank)	Steam	1.85150065
Total		**1.85150065**

Table 4.30 Summary of equipment cost estimation of MEA-based process

	Equipment	Type	Materials	Unit	Size Parameter	size unit	Cost	Spare (15%)	Cost (spare)	Cost Index	Cost(2013)
1	Flue Gas Scrubber	Horizontal Vessel	SS	Scrubber	Dia/H = 2.1336, 3.6576	m	92,908	1.15	106844.2	1.4751434	157,610.52
2	Absorber	Packed	Shell: CS, Packing: SS	Absorber	Dia/H = 2.5908, 25.6032	m	330,591	1.15	380179.65	1.4751434	560,819.51
3	Absorber Pump	Centrifugal	SS	B1	6.277554	m3.kPa/s	13,516	1.15	15543.4	1.4751434	22,928.74
4	Rich/Lean Heat Exchanger	Shell and Tube Floating Head	Tube: SS, Shell: CS	Cross HX	A= 94.346	m2	20,222	1.15	23255.3	1.4751434	34,304.90
5	Stripper	Packed	Shell: CS, Packing: SS	Stripper	Dia/H =1.524, 23.7744	m	158,572	1.15	182357.8	1.4751434	269,003.91
6	Stripper Pre-heater	Heater	CS	B2	2086	kW	59,924	1.15	68912.6	1.4751434	101,655.97
7	Stripper Pump	Centrifugal	SS	B7	1.68616	m3.kPa/s	13,516	1.15	15543.4	1.4751434	22,928.74
8	Condenser	Heater	CS	CONDEN	849.52119	kW	30,199	1.15	34728.85	1.4751434	51,230.03
9	Reflux Tank	Horizontal Vessel	SS	REFLUX	Dia/H = 0.9144, 3.6576	m	21,311	1.15	24507.65	1.4751434	36,152.29
10	Reflux Pump	Centrifugal	SS	B6	0.042306	m3.kPa/s	2,715	1.15	3122.25	1.4751434	4,605.76
11	Absorber Pre-cooler	Heater	CS	COOLER	8606.8939	kW	176,649	1.15	203146.35	1.4751434	29,9670.00
12	Packing	-	SS		135.0289+23.3614	m3	845,700	1.15	972555	1.4751434	1,434,658.1
	TOTAL										**2,995,568.5**

Table 4.31 Summary of equipment cost estimation of IL-based process

	Equipment	Type	Materials	Unit	Size Parameter	size unit	Cost	Spare (15%)	Cost (spare)	Cost Index	Cost(2013)
1	Flue Gas Compressor	Centrifugal	SS	B19	3676.0041	kW	5,064,957	1	5,064,957	1.4751434	7471538.10
2	Flue Gas Cooler	Heater	CS	B20	4589.2974	kW	109,343	1.15	125744.45	1.4751434	185491.100
3	Absorber	Packed	Shell: CS, Packing: SS	B2	Dia/H = 1.524, 21.336	m	155,160	1.15	178434	1.4751434	263215.74
4	Cross Heat Exchanger	Shell and Tube Floating Head	Tube: SS, Shell: CS	B4	A = 22.0299485	m2	11,170	1.15	12845.5	1.4751434	18948.95
5	Flash Tank	Vertical Vessel	SS	B3	Dia/H = 1.0668, 4.572	m	64,949	1.15	74691.35	1.4751434	110180.45
6	Flash Pre-heater	Heater	CS	B1	4610.52797	kW	109,729	1.15	126188.35	1.4751434	186145.91
7	Flash Pump	Centrifugal	SS	B5	50.93596	m3.kPa/s	16,320	1.15	18768	1.4751434	27685.49
8	Absorber Precooler	Heater	CS	B6	1292.5881	kW	41,594	1.15	47833.1	1.4751434	70560.68
9	Heat Exchanger	Shell and Tube Floating Head	Tube: SS, Shell: CS	B7	A = 86.52943	m2	21,913	1	21,913	1.4751434	32324.81
10	Compressor	Centrifugal	SS	B8	1230.41465	kW	1,803,467	1	1,803,467	1.4751434	2660372.51
11	Cooler	Heater	CS	B9	4770.4124	kW	112,620	1	112,620	1.4751434	166130.65
12	Packing	-	SS		38.93556	m3	214,730	1.15	246939.5	1.4751434	364271.18
	TOTAL (engineered equipment)										**1,109,167.8**

Table 4.32 Total capital investment cost of MEA-based process

Total Capital Investment			
1	**Fixed Capital Investment**		**15,397,221**
2	**Working Capital**		**2,666,056**
		Total TCI	**18,063,278**
Direct		**Factor (%)**	**Dollars ($)**
	Purchased Equipment Delivered	1.1	3,295,125
	Purchesed Equipment Installation	0.47	1,407,917
	Instrumentation and Controls (Installed)	0.36	1,078,404
	Piping (Installed)	0.68	2,036,986
	Electrical Systems (Installed)	0.11	329,512
	Building (Including Services)	0.18	539,202
	Yard Improvement	0.1	299,556
	Service Facilities (Installed)	0.7	2,096,897
		Total	**11,083,603**
Indirect	Engineering and Supervision	0.33	988,537
	Construction Expenses	0.41	1,228,183
	Legal Expenses	0.04	119,822
	Contractor's Fees	0.22	659,025
	Contingency	0.44	1,318,050
		Total	**4,313,618**
Working Capital		0.89	2,666,056
		Total	**2,666,056**
	Total Capital Investment ($)		**18,063,278**
	Working Fluid ($)		**31,482**
Total Investment Cost ($)			**18,094,760**

Table 4.33 Total capital investment cost of IL-based process

Total Capital Investment			
1	**Fixed Capital Investment**		**5,701,121**
2	**Working Capital**		**1,597,201**
		Total TCI	**6,688,282**
Direct		**Factor (%)**	**Dollars ($)**
	Purchased Equipment Delivered	1.1	1,220,084
	Purchesed Equipment Installation	0.47	521,308
	Instrumentation and Controls (Installed)	0.36	399,300
	Piping (Installed)	0.68	754,234
	Electrical Systems (Installed)	0.11	122,008
	Building (Including Services)	0.18	199,650
	Yard Improvement	0.1	110,916
	Service Facilities (Installed)	0.7	776,417
		Total	**4,103,921**
Indirect	Engineering and Supervision	0.33	366,025
	Construction Expenses	0.41	454,758
	Legal Expenses	0.04	44,366
	Contractor's Fees	0.22	244,016
	Contingency	0.44	488,033
		Total	**1,597,201**
Working Capital		0.89	987,159
		Total	**987,159**
	Total Capital Investment ($)		**6,688,282**
	Additional Equipment Cost ($)		**10,330,366**
	Working Fluid ($)		**398,137**
Total Investment Cost ($)			**17,416,785**